Acta Pharmaceutica Sinica B 2026;16(2):1009−1021

Chinese Pharmaceutical Association
Institute of Materia Medica, Chinese Academy of Medical Sciences

Acta Pharmaceutica Sinica B

www.elsevier.com/locate/apsb
www.sciencedirect.com

ORIGINAL ARTICLE

# Hyperimonates A and B, a pair of unprecedented polyprenylated acylphloroglucinols from *Hypericum monogynum*: Structural elucidation, total synthesis, and lipid-lowering activity

**Chunmao Yuan[a,†], Zhao Liu[b,c,†], Lei Huang[a,†], Chunxiang Mei[b,c], Yanrong Zeng[a], Yanmei Li[b,c], Yang Chen[b,c], Hongji Wang[a], Lan Yang[b,c], Xiaojiang Hao[a,d,*], Shuzhong He[b,c,*]**

[a]*State Key Laboratory of Discovery and Utilization of Functional Components in Traditional Chinese Medicine, Guizhou Medical University & Natural Products Research Center of Guizhou Province, Guiyang 550014, China*
[b]*School of Pharmaceutical Sciences, Guizhou University, Guiyang 550025, China*
[c]*Guizhou Engineering Laboratory for Synthetic Drugs, Guizhou University, Guiyang 550025, China*
[d]*State Key Laboratory of Phytochemistry and Natural Medicines, Kunming, Institute of Botany, Chinese Academy of Sciences, Kunming 650201, China*

Received 22 April 2025; received in revised form 22 June 2025; accepted 15 July 2025

**KEY WORDS**

Natural products;
*Hypericum monogynum*;
Polyprenylated acylphloroglucinols;
Isolation and structural elucidation;
Asymmetric total synthese;
Lipid-lowering activity;

**Abstract** Hyperimonates A (**1**) and B (**2**), two minor polycyclic polyprenylated acylphloroglucinols (PPAPs) with unprecedented hexahydro-1*H*-cyclopenta[*c*]furan-1-one and 2-oxabicyclo[2.2.1]heptane ring system were isolated from *Hypericum monogynum*. To obtain adequate materials for biological research, the asymmetric total syntheses of **1** and **2** were completed from commercially available geraniol *via* a bioinspired strategy that features an Au(I)-catalyzed carbometallic cascade cyclization and a Mn (III)/Cu(II) mediated oxidative radical cyclization as vital steps. Biological study implied that compound **1** showed excellent lipid-lowering activity *in vitro via* inhibiting two signaling pathways, Notch and PPAR, further verified by non-alcoholic fatty liver disease (NAFLD) zebrafish model. These findings provide a new structural template for the treatment of NAFLD and asymmetric synthetic approaches could also facilitate further evaluation for drug development.

*Corresponding authors.
E-mail addresses: haoxj@mail.kib.ac.cn (Xiaojiang Hao), szhe@gzu.edu.cn (Shuzhong He).
†These authors made equal contributions to this work.

Peer review under the responsibility of Chinese Pharmaceutical Association and Institute of Materia Medica, Chinese Academy of Medical Sciences.

https://doi.org/10.1016/j.apsb.2025.10.008

Mechanistic study;
Anti-NAFLD



## 1. Introduction

Non-alcoholic fatty liver disease (NAFLD), characterized by excessive fat accumulation in hepatocytes, has emerged as a leading cause of chronic liver disease worldwide[1]. The global prevalence of NAFLD in adults is estimated at 30.2%, rising to 70% among patients with type II diabetes mellitus[1,2]. Clinically, various lipid-lowering drugs, such as resmetirom, atorvastatin, and pioglitazone, are used to treat NAFLD[2,3]. However, these drugs are often associated with side effects, including diarrhea, stomach pain, constipation, and nausea. Natural products (NPs) have long been recognized as valuable sources of inspiration for drug discovery[4]. Consequently, identifying new anti-NAFLD lead compounds from natural sources with minimal or no side effects presents a promising approach. A significant challenge, however, is that many bioactive NPs are isolated in small quantities, limiting their potential for further *in vitro* and *in vivo* mechanistic studies. To address this issue, the "Isolation−Synthesis−Functionality" strategy has been developed[5−7], offering a new pathway to accelerate the discovery of anti-NAFLD lead compounds.

Polycyclic polyprenylated acylphloroglucinols (PPAPs) are biogenetically derived from acylphloroglucinol cores extensively modified with prenyl, geranyl, or more complex side chains[8−9]. To date, over 600 PPAP derivatives have been identified from the Guttiferae family[8−9]. These compounds exhibit unique structures and remarkable bioactivities, including antidepressant, anti-inflammatory, AChE inhibitory, Cav3.1 agonist, lipid-lowering, and anti-Alzheimer's properties[10−15]. Notably, hyperforin (Fig. 1), the most well-known PPAP, is recognized as the primary antidepressive component in St. John's wort (*Hypericum perforatum*) and GNC St. John's Wort Extract Capsules[8]. Due to their structural complexity and potential as pharmaceutical leads, PPAPs are highly attractive in the areas of NPs, medical chemistry, and total synthesis[16−21].

Mining novel types of NPs from traditional Chinese Medicine is a promising way to develop new lead compound for the treatment of NAFLD. *Hypericum monogynum* Linn., a medicinal plant, was applied to cure hepatitis, conjunctivitis, and acute laryngopharyngitis[13]. Thus, as part of our ongoing research, this plant was applied for our study, which obtained a pair of rare polycyclic polyprenylated acylphloroglucinols (PPAPs). Structurally, compounds **1** and **2** feature rare hexahydro-1*H*-cyclopenta[*c*]furan-1-one and 2-oxabicyclo[2.2.1]heptane ring systems (Fig. 1A). However, due to the limited quantities obtained, further evaluation of their anti-NAFLD activity was hindered. To address this, we report the isolation, structural elucidation, asymmetric total synthesis, and *in vitro* and *in vivo* anti-NAFLD activity of these compounds.

## 2. Results and discussion

### 2.1. The structure elucidation of compounds *1* and *2*

Hyperimonate A (**1**) has a molecular formula of $C_{20}H_{30}O_4$ with six indices of hydrogen deficiency (IHDs) according to the protonated ion peak at *m/z* 335.2219 ($[M + H]^+$ Calcd. for $C_{20}H_{31}O_4$: 335.2217) in the high-resolution electrospray ionization mass spectroscopy (HR-ESI-MS). Detailed analysis of the $^1H$ and $^{13}C$ NMR data (Supporting Information Table S1) implied that compound **1** was a PPAP with a tetracyclic structure. According to the $^1H$-$^1H$ COSY spectrum, the following two partial structures with bold bonds were constructed: C-4−C-8 and C-13−C-17 (Fig. 1B). In the HMBC spectrum, the key correlations of Me-10 with C-3, C-4, and C-7; gem-dimethyl (Me-11 and Me-12) with C-8 and C-9; and $H_2$-13 with C-1, C-2, C-3, and C-8 were observed. Furthermore, a γ-lactone ring was deduced based on two characteristic chemical shifts, C-9 ($\delta_C$ 83.5) and C-1 ($\delta_C$ 172.1), and the gross structure of unit A was constructed. Similarly, the HMBC correlations from Me-22 to C-14, C-17, and C-18 and from gem-dimethyl (Me-20 and Me-21) to C-15 and C-19, along with the downfield-shifted signals at C-18 ($\delta_C$ 85.4) and C-19 ($\delta_C$ 79.7), established unit B. Thus, the planar structure of **1** was

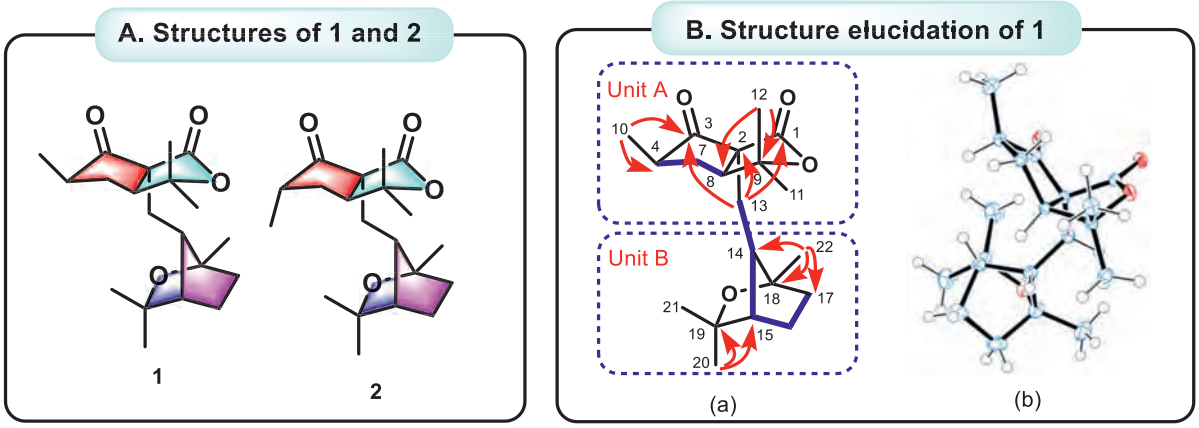


**Figure 1** Structures of hyperimonates A (**1**) and B (**2**) and their structural elucidation.

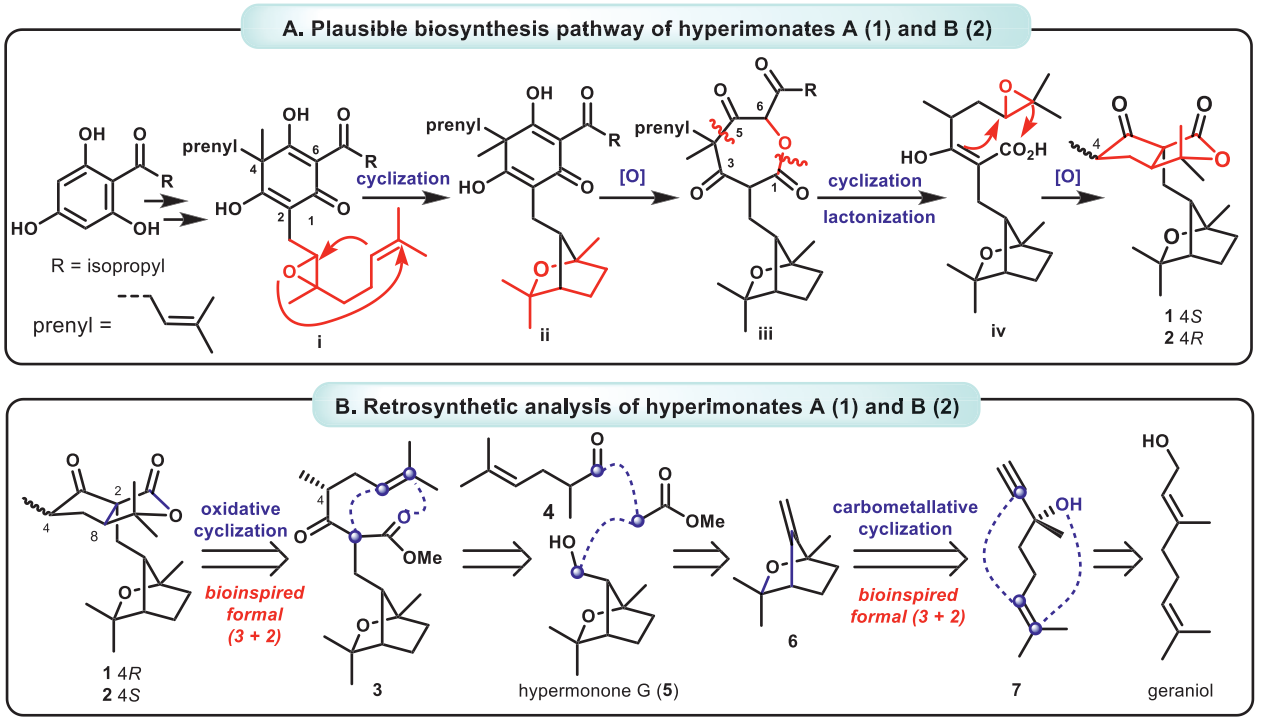


**Scheme 1** Plausible biosynthetic pathways and retrosynthetic analysis of hyperimonates A (**1**) and B (**2**).

established. However, we could not determine its relative configuration due to the lack of sufficient key NOESY correlations. Fortunately, suitable crystals of **1** were obtained from MeOH and analyzed *via* single-crystal X-ray diffraction (Supporting Information Fig. S1), which further confirmed its planar structure and absolute configuration (Fig. 1B). The structure elucidation of compound **2** is described in the Supporting Information (Supporting Information Figs. S2 and S3).

To ascertain whether the two novel compounds (**1** and **2**) were inherent components of the plant, liquid chromatography-mass spectrometry (LC−MS) analysis was conducted for the crude extract and two compounds (Supporting Information Figs. S4−S6). The results implied that these two compounds were indeed present in the crude extract of the plant. Interestingly, compounds **1** and **2** were interconvertible slowly when stored in methanol (MeOH) at room temperature. In order to investigate the transformative conditions, compound **1** was submitted to thermodynamic, acidic (TsOH) and basic ($Et_3N$) conditions. As a result, temperature was found to be the main factor, and the mutual transformation rate of compounds **1** and **2** increased when one of the two compounds was stirred in MeOH at higher temperatures (Supporting Information Fig. S7-1−S7-2).

### 2.2. *Asymmetric hypothesis and retrosynthetic analysis*

Compounds **1** and **2** were identified as a new class of PPAPs, featuring an unprecedented 5/5-5/5 ring system. Based on PPAPs analysis, a plausible biogenetic pathway for these compounds is proposed in Scheme 1A. Initially, similar to other PPAPs, intermediate **i** could be biosynthesized from acylphloroglucinol through the action of

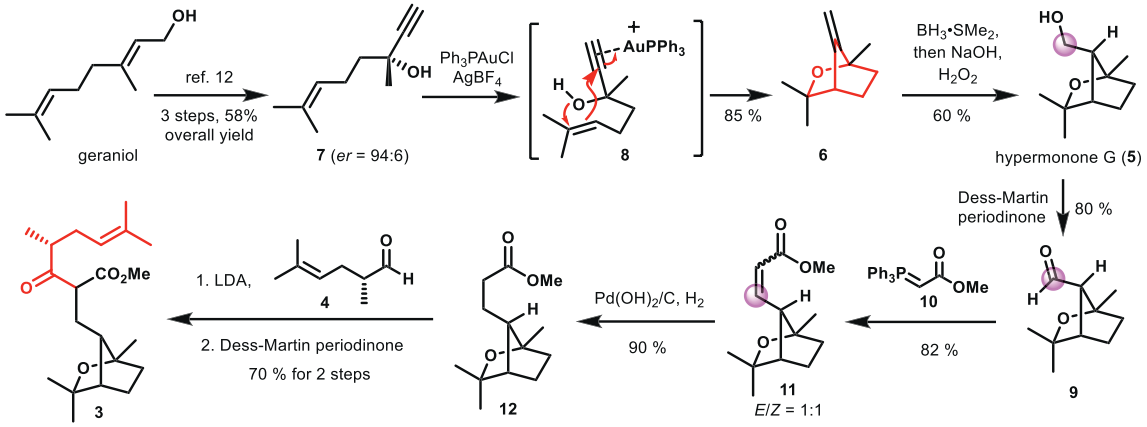


**Scheme 2** Asymmetric synthesis of intermediate 3 *via* a carbometallative formal (3 + 2) cyclization.

**Table 1** Oxidative radical cascade cyclization.

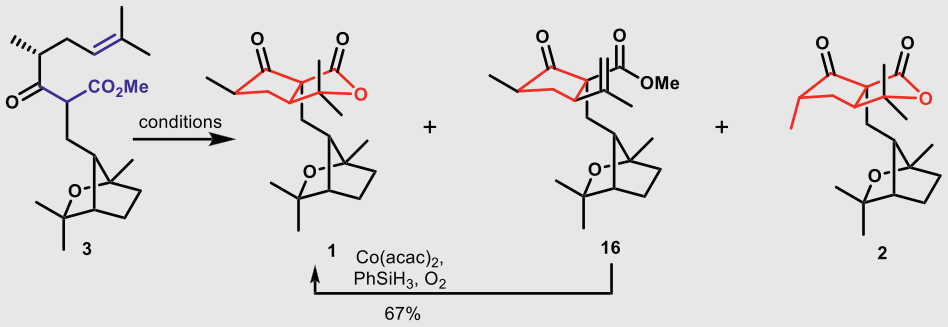


| Entry | Conditions | Yield[a] (%) | | |
|---|---|---|---|---|
| | | 1 | 16 | 2 |
| 1 | $Fe(ClO_4)_3$, $CH_3CN$, 50 °C | —[b] | | |
| 2 | $Mn(OAc)_3$, AcOH 80 °C | —[b] | | |
| 3 | $Mn(OAc)_3$, $Cu(OAc)_2$, AcOH, 40 °C | —[b] | | |
| 4 | $Mn(OAc)_3$, $Cu(OAc)_2$, EtOH, 80 °C | —[b] | | |
| 5 | $Mn(OAc)_3$, $Cu(OAc)_2$, $CH_3CN$, rt | —[b] | | |
| 6 | $Mn(OAc)_3$, $Yb(OTf)_3$, TFE, rt | 14 | 4 | 0 |
| 7 | $Mn(OAc)_3$, $Cu(OTf)_2$, TFE, 80 °C | 10 | 0 | 0 |
| 8 | $Mn(OAc)_3$, $Cu(OTf)_2$, $CH_3CN$, 80 °C | 37 | 18 | 4 |
| 9 | $Mn(OAc)_3$, $Cu(OTf)_2$, $CH_3CN$, 40 °C | 55 | 20 | 5 |

[a]Isolated yield of the indicated products.
[b]Decomposition of the substrate.

isopentenyl and methyl transferases, as well as oxidase[8,9]. This intermediate could undergo epoxide opening and intramolecular etherification cyclization to generate intermediate **ii**, followed by Baeyer-Villiger oxidation to obtain lactone **iii**. After undergoing ring cleavage *via* saponification and retro-Aldol-type fragmentation, the 7-membered lactone experiences alkene epoxidation to form intermediate **iv**. The epoxide opening-induced cyclization of **iv** and subsequent lactonization could generate compounds **1** and **2** as the final products.

Given that the isolated amounts of **1** (4.2 mg) and **2** (3.5 mg) are not sufficient for further bioassay studies, we initiated a project to develop an efficient synthetic strategy for these NPs. Our synthetic strategy features two bioinspired formal (3 + 2) annulations for the rapid construction of two bicyclic systems (Scheme 1B). In retrosynthesis, the γ-lactone ring was first disassembled in a retro (3 + 2) manner, mimicking the process in which β-keto ester (**iv**) could be converted to **1** and **2** in the biosynthesis pathway (Scheme

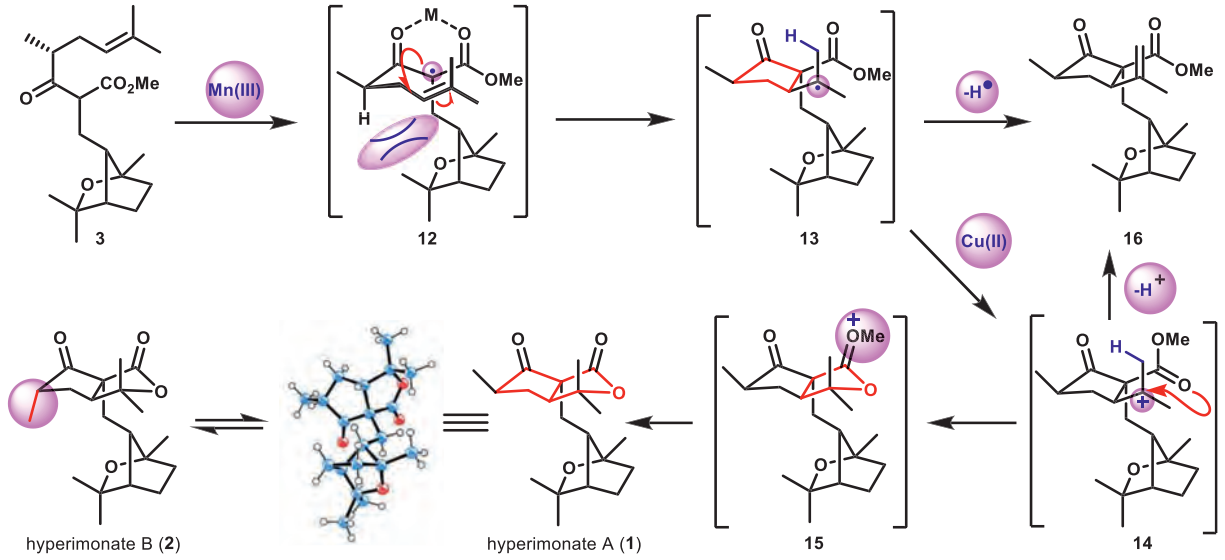


**Scheme 3** Possible reaction process of the formal (3 + 2) radical cyclization.

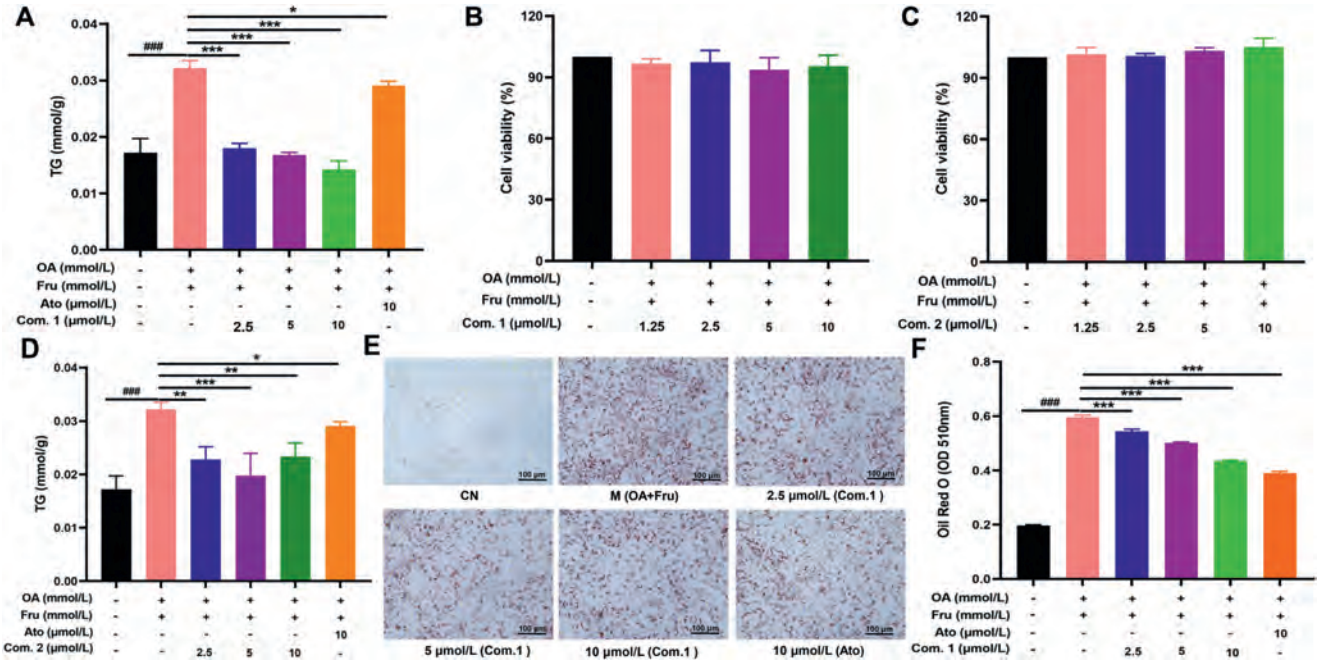


**Figure 2** Effects of compounds **1** and **2** on lipid accumulation in OA/Fr-induced HepG2 cells. (A−D) Effects of compounds **1** and **2** on the accumulation of TG in OA/Fr-induced HepG2 cells and their toxicity. (E, F) Lipid accumulation was observed for com. **1** with ORO staining. Results are expressed as the mean ± standard deviations (SD) ($n = 3$), scale bar = 100 μm $^{\#\#}P < 0.01$ and $^{\#\#\#}P < 0.001$ compared with the control group; $^{**}P < 0.01$ and $^{***}P < 0.001$ compared with the model group.

1). In the forward direction, we envisioned that metal-mediated oxidative radical formation could initiate a cascade cyclization to construct the cyclopenta[*c*]furanone in one step[22]. We expected that C-4 chirality plays an important role in controlling the stereochemistry at C-2 and C-8 in this process. *β*-Keto ester **3** was divided into three fragments, methyl acetate, chiral enal **4** (with both *R*- and *S*-configurations), and hypermonone G (**5**), a natural product also isolated from *H. monogynum* by our group. Fragment coupling could be achieved by sequential Aldol reaction and *α*-alkylation of methyl acetate. The key fragment, hypermonone G (**5**), could then

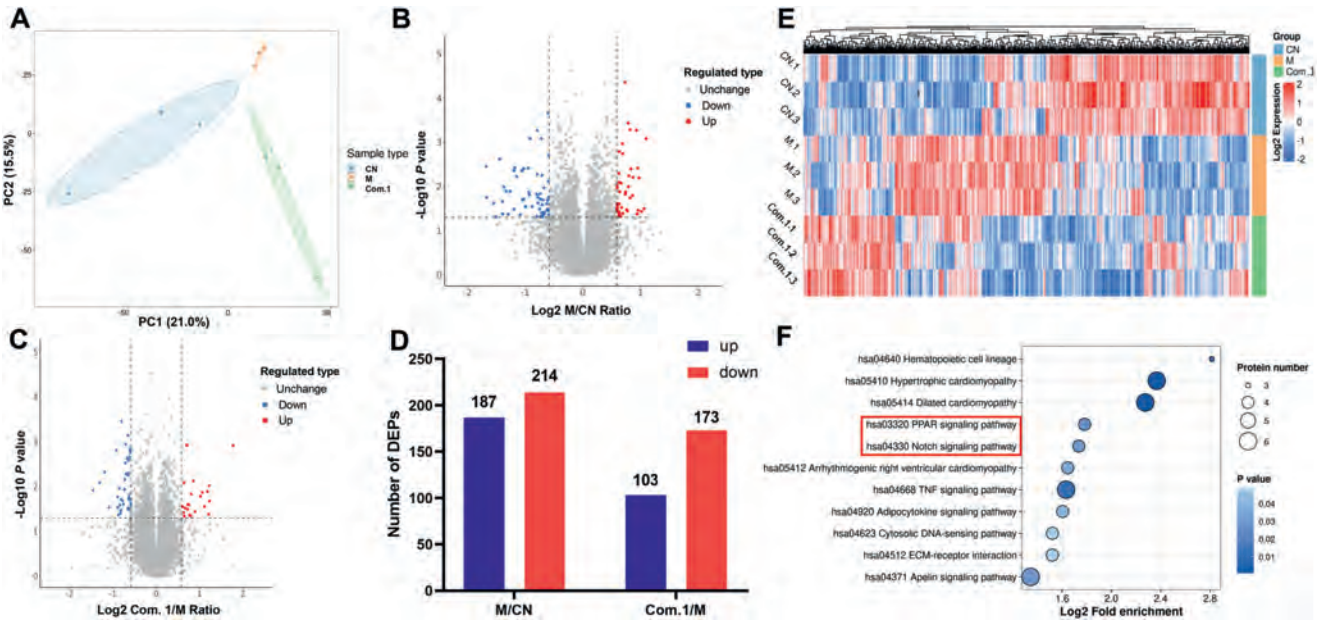


**Figure 3** The mechanistic study of compound **1** on the lipid accumulation in HepG2 cells. (A−F) Proteomic study when treated with **1**. (A) Principal component analysis (PCA). (B) Model (M) *vs*. control (CN) differentially expressed proteins (DEPs) volcano diagram. (C) Com. **1** *vs*. M DEPs volcano diagram. (D) DEPs between M and CN group, as well as com. **1** and M. group. (E) Clustering heat map of differential protein expression in the three groups. (F) KEGG pathway enrichment analysis.

be traced back to alkene **6** *via* diastereoselective hydroboration-oxidation. Bicycle **6** may arise from a carbometallative formal (3 + 2) annulation from precursor **7**[23–26] (Supporting Information Table S2), which is inspired by the biosynthetic process from **i** to **ii**. Intermediate **7**, a known material, can be prepared from geraniol.

### 2.3. *Total synthesis of hyperimonates A and B*

Our synthesis of hyperimonate A (**1**) commenced with the enantioselective synthesis of enynol **7** (Scheme 2)[27], which was readily prepared in decagram scales from genraniol by Sharpless asymmetric epoxidation, chlorination, and then BuLi-promoted double elimination (3 steps, 58% yield, *er* = 94:6)[12]. To realize the first bioinspired formal (3 + 2) design, enyol **7** was subjected to several Au(I) conditions to carry out carbometallic cascade cyclization[28]. Gratifyingly, after treatment with $PPh_3AuCl/AgBF_4$, bridged oxabicycle **6** was successfully obtained in 85% yield. The key to producing this high yield was using toluene as the solvent. The reaction mechanism may involve a cationic Au(I)-induced carbometallic addition of the terminal alkyne by the trisubstituted alkene, followed by interception of the newly formed tertiary carbocation with the hydroxyl group. With the oxabicyclic system established, a hydroboration-oxidation procedure provided hypermonone G (**5**) as a single diastereoisomer. This stereochemical outcome could be attributed to the steric effect of the C-20 methyl group, which forces the boration reagent to access from the opposite side.

With key fragment **5** in hand, we explored the installation of the remaining atoms to construct cyclopenta[*c*]furanone (Scheme 2). We initially attempted to realize alkylation between methyl acetate or its *β*-keto ester derivative and iodinated or sulfonylated **5**. However, these fragment couplings were unsuccessful, presumably due to the strict requirement of orbital overlap in $S_N2$ reactions as well as the steric effect of the bulky bicycle moiety. As a solution, the primary alcohol was oxidized to the corresponding aldehyde **9**, which was then subjected to nucleophilic addition and condensation. Although direct Knoevenagel condensation with *β*-keto esters failed to yield the desired coupling product, **9** reacted well with Wittig reagent **10** in refluxed benzene to provide olefination product **11** as an *E*/*Z* mixture. After the double bond was hydrogenated, methyl ester **12** was deprotonated by LDA to participate in an Aldol reaction with chiral

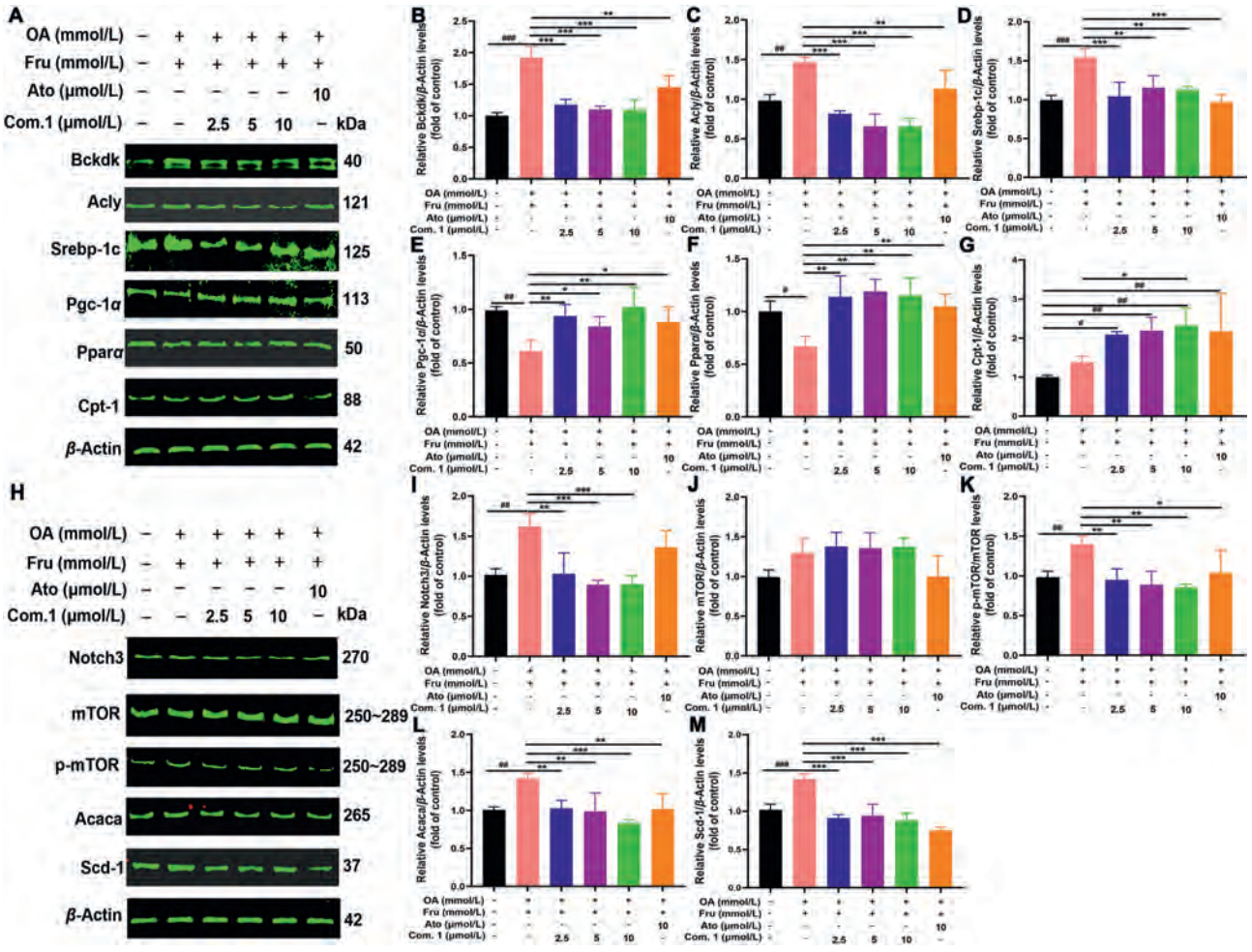


**Figure 4** Effect of compound **1** on the expression levels of proteins in OA/Fro-induced HepG2 cells. (A, G) The expression levels of proteins were analyzed by Western blot in OA/Fro-induced HepG2 cells after treatment with compound **1** for 48 h. (B−F, H−M) Schematic diagram showing the mechanism of the protective effect of compound **1** on lipid metabolism disorder. Results are expressed as the mean ± SD ($n$ = 3). $^{\#}P < 0.05$, $^{\#\#}P < 0.01$ and $^{\#\#\#}P < 0.001$ compared with the control group; $^{*}P < 0.05$, $^{**}P < 0.01$, and $^{***}P < 0.001$ compared with the model group.

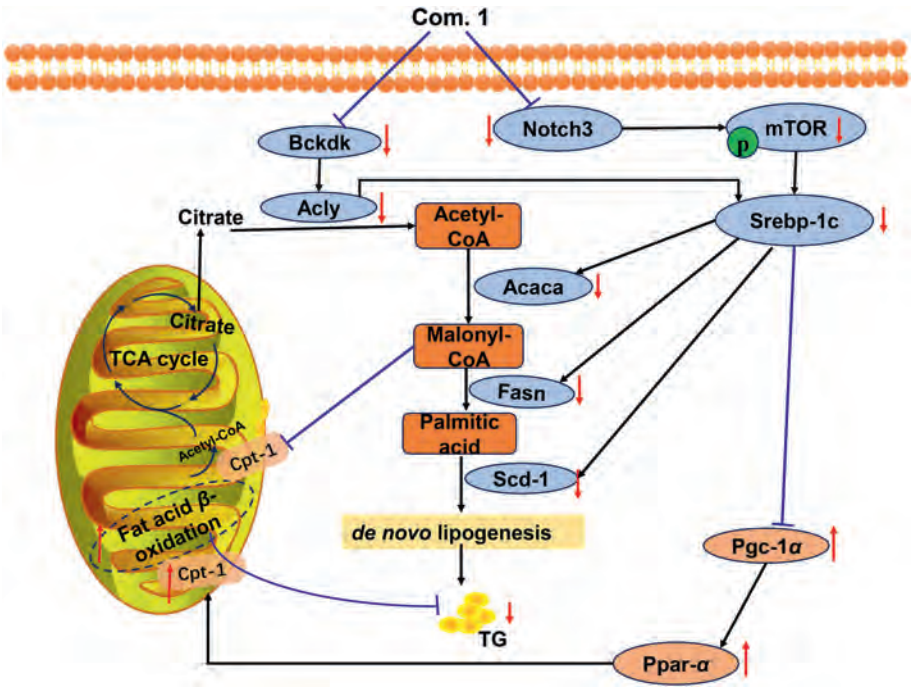


**Figure 5** Schematic diagram showing the mechanism of the protective effect of Com. **1** on lipid metabolism disorder.

aldehyde **4**, which could be readily prepared in 2 steps from propionyl chiral oxazolidinone. A subsequent Dess-Martin oxidation then furnished $\beta$-keto ester **3** in good yield.

At this stage, the remaining task is to construct the cyclopenta [*c*]furanone by the second formal (3 + 2) design. To realize the radical cyclization-lactonization cascade, we initially employed $Fe(ClO_4)_3$ as the oxidant, which was reported to participate in a similar ring construction process by Yang and coworkers (Table 1, entry 1)[29]. However, these conditions and the other Fe(III) oxidants only led to decomposition of our substrate[30,31]. Then, we shifted the reaction conditions to the well-studied Mn(III) system[32]. Typical Mn(III) oxidative conditions, such as heating with $Mn(OAc)_3$ or adding $Cu(OAc)_2$ as the co-oxidant, caused the substrate to decompose[33,34]; while the usage of $Mn(OAc)_3$ and Yb $(OTf)_3$ was a fruitful effort (Table 1, entries 2−5; Supporting Information Table S3)[35,36]. Under these conditions, the desired natural product **1** was obtained in 14% yield, and a monocyclized side product **16** was obtained in 4% yield (Table 1, entry 6). Encouraged by these findings, we investigated the use of different additives. Although changing the additive to $Cu(OTf)_2$ decreased the reaction efficiency (entry 7), further study on different solvents demonstrated that Burton's conditions ($Mn(OAc)_3$, $Cu(OTf)_2$, $CH_3CN$, 80 °C) could significantly improve the yield of **1** to 37% (Table 1, entry 8)[37,38]. Furthermore, when a lower reaction temperature was used (40 °C), hyperimonate A was obtained in 55% yield, together with 20% yield of **16** (entry 9). With these conditions, we also isolated small amounts of hyperimonate B (**2**), which may be generated from **1** *via* epimerization during the heating process (entries 8, 9). Additionally, monocyclized product **16** was found to be easily transformed to **1** by Mukaiyama hydration[39,40]. The NMR spectral data of synthesized **1** and **2** were in good accordance with those of the isolated compounds (Supporting Information Tables S4 and S5), and the structure of our synthetic material **1** was unambiguously determined *via* X-ray crystallography.

The mechanism of this formal (3 + 2) cyclization presumably involves initial Mn(III) oxidation of the $\beta$-keto ester to generate radical **12** (Scheme 3), which likely undergoes cyclization with the trisubstituted alkene to tertiary radical **13**. This radical can then be oxidized by Cu(II) to carbocation **14**, which can be sequentially intercepted by the spatially adjacent ester group, yielding NPs **1** and **2**. Otherwise, radical **13** or carbocation **14** can also undergo direct $\beta$-H elimination to generate side product **16**. Notably, the reaction is highly diastereoselective, and no other stereochemical isomer was isolated from the reaction mixture. This stereochemistry may result from the bulky oxabicyclo[2.2.1] heptane moiety, which may play an important role in securing the pseudo-equatorial position of the C-10 methyl group and forcing the alkenyl group to adopt an s-trans conformation in **12**. As a result, the isopropyl group and the methyl ester in intermediate **13** exhibited a *cis* configuration.

### 2.4. *Lipid-lowering activity of hyperimonates A and B*

With adequate amounts of **1** and **2** available, they were evaluated for their lipid-lowering effects on a hepatic steatosis model induced by oleic acid (OA) and fructose (Fro) in HepG2 cells[41-43]. As shown in Fig. 2A and C, both compounds **1** and **2** (Com. **1** and **2**) did not exhibit toxicity on HepG2 cells at concentrations from 1.25 to 10 μmol/L. At the same time, compounds **1** and **2** exhibited concentration-dependent inhibition of triglyceride (TG) production caused by OA/Fro at three different concentrations (2.5, 5, and 10 μmol/L) (Fig. 2B and D), higher than the lipid-lowering drug atorvastatin (Ato). Further oil red O (ORO) staining experiment was conducted in HepG2 cells, and the results were consistent with the TG inhibition of compound **1** (Fig. 2E and F).

To further investigate the mechanism of compound **1**, we conducted proteomics to find the protein expression profile of model cells (OA/Fr-induced HepG2 cells) closely related to the

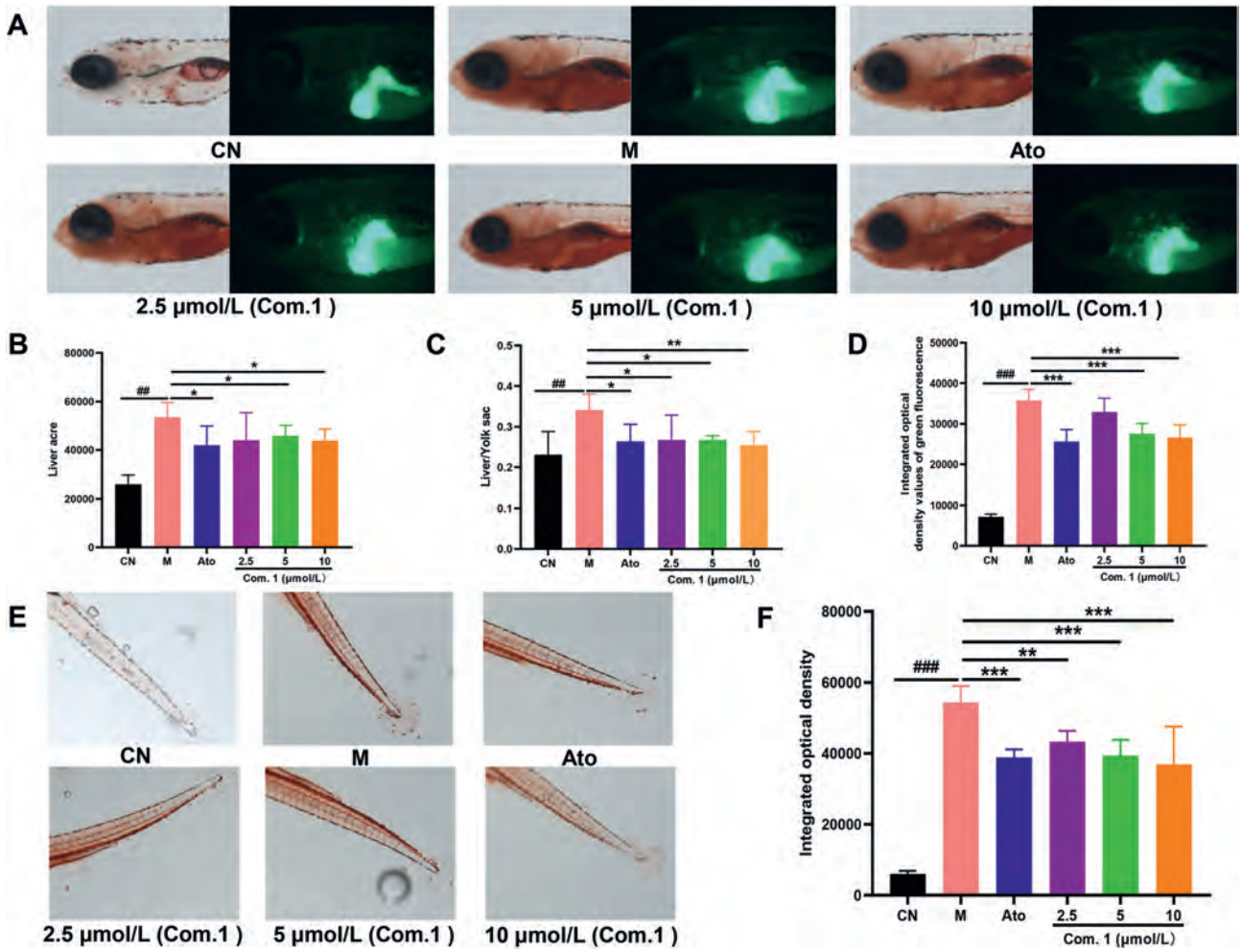


**Figure 6** Effects of compound **1** on NAFLD induced by fructose and egg yolk in zebrafish. (A) Representative images of the lateral view were obtained from vehicle (0.1% DMSO) or drug-exposed zebrafish larvae (Com. **1**: 2.5−10 μmol/L or Ato: 10 μmol/L). Green and red dotted lines indicate the outer margins of the liver and yolk sac, respectively. (B−D) Liver and yolk sizes obtained from com. **1** and Ato exposed zebrafish larvae were quantitated. (E, F) Oil Red O staining was performed to observe changes in lipid accumulation in the tail vasculature of zebrafish. Results are expressed as the mean ± SD ($n = 10$). $^{\#\#}P < 0.01$ and $^{\#\#\#}P < 0.001$ compared with the CN group; $^{*}P < 0.05$, $^{**}P < 0.01$, and $^{***}P < 0.001$ compared with the M group.

lipid-lowering activity. Results show that the principal component analysis (PCA) plot exhibited a clear separation among the three groups where compound **1** group was located much closer to the control group (CN.) than the model group (M.) alongside PC1, indicating compound **1** group has a higher similarity to the CN. group, rather than the M. group (Fig. 3A). Differentially expressed proteins (DEPs) were filtered (M. *vs*. CN., Com. **1** *vs*. M.) by the *P*-adjusted value ($P < 0.05$), and fold change (absolute FC $> 1.2$) was displayed in Fig. 3B and C. And 103 up-regulated proteins and 173 down-regulated proteins were observed in the OA/Fro-induced HepG2 cells after compound **1** treatment compared with the model group (Fig. 3D). Among them, 60 proteins were commonly altered. Heatmap analysis showed that intervention with compound **1** reversed the abnormal expression levels of 60 proteins in metabolism disorder cells caused by OA/Fro, returning them to near normal levels (Fig. 3E). Then, a KEGG pathway enrichment analysis of DEPs was performed. The results demonstrated that the therapeutic mechanism of compound **1** in OA/Fro-induced HepG2 cells primarily involves modulation of multiple signaling pathways, such as the regulation of hematopoietic cell lineage, hypertrophic cardiomyopathy, dilated cardiomyopathy, PPAR signaling pathway, Notch signaling pathway, arrhythmogenic right ventricular cardiomyopathy, TNF signaling pathway, adipocytokine signaling pathway, cytosolic DNA-sensing pathway, ECM-receptor interaction, and apelin signaling pathway ($P < 0.05$, Fig. 3F). Among these, the PPAR and Notch signaling pathways—known to play critical roles in lipid metabolism and NAFLD progression[44,45]—were selected for further mechanistic investigation.

On the one hand, branched-chain ketoacid dehydrogenase kinase (Bckdk), a key upstream regulator in the PPAR signaling pathway under NAFLD conditions, was significantly upregulated. What's more, Bckdk was considered to be a potential target for the treatment of NAFLD, and several inhibitors were designed and synthesized[46]. Its upregulation enhanced the expression of lipogenic proteins (Acly and Srebp-1c) while concurrently inhibiting the expression of key fatty acid oxidation regulators (Ppar$\alpha$ and Cpt-1)[47]. In our study, OA/Fro-induced hepatic steatosis

significantly upregulated the expression of lipogenic proteins, with Bckdk, Acly, and Srebp-1c increasing by 92.01%, 49.17%, and 55.30%, respectively, compared to the control group (Fig. 4). Conversely, several fatty acid oxidative proteins (Pgc-1$\alpha$, Ppar$\alpha$, and Cpt-1) were significantly downregulated in the steatosis group (Fig. 4). When treated with compound **1**, the expression of Bckdk and Acly were reduced in a dose-dependent manner, and subsequently down-regulated the proteins of Pgc-1, Ppar$\alpha$, and Cpt-1. Moreover, Srebp-1c, a key transcription factor for *de novo* fatty acid synthesis[48], was increased when treated with compound **1** (Fig. 4). Notably, the lipid-lowering efficacy of compound **1** was comparable to, or superior to, that of the positive control atorvastatin (Ato), demonstrating its significant therapeutic potential against OA/Fro-induced hepatic steatosis.

On the other hand, the Notch signaling pathway begins with the interaction between delta-like protein receptor or Jag1 receptor and Notch receptors 1−4, promoting *de novo* lipogenesis *via* mTOR/Srebp-1c, which leads to lipid accumulation in the liver and the occurrence of NAFLD[44,48]. Among these, Notch 3 is significantly upregulated due to glucolipid metabolism disorders, and thus the lipid synthesis related proteins (Srebp-1c, Acaca, and Scd-1) were also increased[49]. Consistent with previous reports, our study found that the expression of Notch 3 and *p*-mTOR proteins was higher by 59.54% and 42.10%, and the expressions of Srebp-1c, Acaca, and Scd-1 were down-regulated by 55.30%, 41.04%, and 39.61%, respectively, in the OA/Fro-induced hepatic steatosis group compared with that in the control group (Fig. 4). When treated with compound **1**, the expressions of Notch 3 and *p*-mTOR were significantly decreased, prohibiting the lipid synthesis-related proteins (Srebp-1c, Acaca, and Scd-1) (Fig. 4). In summary, compound **1** exhibited good inhibitory effects on PPAR and Notch signaling pathways *via* prohibiting two vital proteins, Bckdk and Notch 3, and induced subsequent changes of fatty acid oxidative and lipid synthesis related proteins (Fig. 5).

Zebrafish have emerged as an important model for studying lipid metabolism disorders and NAFLD pathogenesis[50−53]. To evaluate the lipid-lowering activity of compound **1** *in vivo*, the nonalcoholic fatty liver disease (NAFLD) zebrafish (Tg: cy3-EGFP) model was established by feeding fructose and egg yolk. As shown in Fig. 6A−D, the liver size of NAFLD zebrafish was gradually decreased when treated with concentrations of compound **1** ranging from 2.5 to 10 μmol/L, as indicated by the liver area, liver/yolk sac ratio, and green fluorescent intensity analysis. Additionally, ORO staining showed that the optical density of the NAFLD zebrafish tail in the compound **1** group was obviously reduced in a dose-dependent manner compared to the model group (Fig. 6 E and F). These results suggest that compound **1** can decrease the lipid content and liver size of NAFLD zebrafish induced by fructose and egg yolk, which was comparable to the positive drug atorvastatin (10 μmol/L).

## 3. Conclusions

In summary, hyperimonates A and B (**1** and **2**), the first PPAP featuring a rare 5/5-5/5 ring system, were isolated and characterized in low quantities from the flowers of *H. monogynum*. Due to the presence of two bicyclic systems connected by a methylene group, compounds **1** and **2** were interconvertible at elevated temperatures. Inspired by their biosynthetic pathway, an asymmetric total synthesis of **1** and **2** was achieved in 11 steps from commercially available geraniol. The key oxabicyclo[2.2.1]heptane system was constructed through a formal carbometallic (3 + 2) cascade cyclization in one step, while the cyclopenta[*c*]furanone ring was formed *via* an oxidative formal (3 + 2) radical cascade. Compound **1** demonstrated significant suppression of lipid accumulation by inhibiting the Notch and PPAR signaling pathways *in vitro*, outperforming atorvastatin. This effect was further validated using a NAFLD zebrafish model. To the best of our knowledge, this is the first report of PPAPs with potential anti-NAFLD activity through the inhibition of two critical proteins, Notch 3 and Bckdk. In future work, the HFD-induced NAFLD mouse model will be applied to further validate efficacy, pharmacokinetics, and long-term safety. This study exemplifies the "Isolation−Synthesis−Functionality" strategy in natural product research. Compounds **1** and **2** represent novel structural templates for the development of anti-NAFLD drugs. The bioinspired total synthesis of these unprecedented PPAPs enables further evaluation for drug development.

## 4. Experimental

### 4.1. General experimental procedures

See Supporting Information

### 4.2. Plant materials

The flowers of *H. monogynum* were collected in June 2018, in Guiyang, Guizhou Province of China, which were identified by Dr. Wei Gu. A voucher specimen (H20180601) was deposited at the Natural Products Research Center of Guizhou Province.

### 4.3. Extraction and isolation

The air-dried flowers of *H. monogynum* (9 kg) were extracted with MeOH at room temperature to obtain 1.2 kg of crude residue, which was subjected to silica gel chromatography eluted with petroleum ether/EtOAc (100:0 → 0:100, *v*/*v*) and then $CHCl_3$/MeOH to yield seven major fractions (A−G). Fraction D (220 g) was fractionated by a RP-C18 column chromatography eluted with a gradient of MeOH/$H_2O$ (40:60 → 100:0) to give five subfractions (D1−D5). Fraction D3 (26 g) was loaded on a silica gel column (petroleum ether/acetone, 100:0 → 0:100, *v*/*v*) to afford six fractions (D1a−D1f). Subsequently, fraction D1e (1.6 g) was repeatedly chromatographed over silica gel and Sephadex LH-20 column to afford a major component, which was further purified by semi-preparative HPLC (MeOH-$H_2O$, 58:42, *v*/*v*) to afford **1** (4.2 mg) and **2** (3.5 mg), respectively.

#### 4.3.1. Hyperimonate A (*1*)

Colorless crystals; m.p. 131−132 °C; $[\alpha]_D^{25}$ +34.00 (*c* 0.20, MeOH); UV (MeOH) $\lambda_{max}$ 203 and 273 nm; IR (KBr) $\nu_{max}$ 1764, 1729, 1455, 1378, 1267, 1168, 948, 906 $cm^{-1}$; CD (MeOH) $\lambda$ ($\Delta\varepsilon$) 221 (+30.50), 262 (+1.11), 280 (+2.19), 309 (−4.16); for $^1H$ NMR and $^{13}C$ NMR data, see Table S1; HR-ESI-MS *m/z* 335.2219 ($[M+H]^+$, Calcd. for $C_{20}H_{31}O_4$: 335.2217).

#### 4.3.2. Hyperimonate B (*2*)

White amorphous solid; $[\alpha]_D^{25}$−10.00 (*c* 0.20, MeOH); UV (MeOH) $\lambda_{max}$ 203 and 278 nm; IR (KBr) $\nu_{max}$ 1770, 1729, 1459, 1378, 1268, 1154, 958, 909 $cm^{-1}$; CD (MeOH) $\lambda$ ($\Delta\varepsilon$) 221 (−0.87), 239 (−2.11), 304 (+57.08); for $^1H$ NMR and $^{13}C$ NMR

data, see Table S1; HR-ESI-MS *m/z* 357.2037 ($[M + Na]^+$, Calcd. for $C_{20}H_{30}O_4Na$: 357.2036).

### 4.4. X-ray crystallographic analyses

Crystals of compound **1** were obtained by using the solvent vapor diffusion method. The single-crystal X-ray diffraction data were recorded on a Bruker D8 QUEST instrument (Cu K$\alpha$ radiation). Crystals were kept at 100.(2) K during data collection. The crystallographic data of those compounds in standard CIF format were deposited at the Cambridge Crystallographic Data Centre. The data can be accessed free of charge at http://www.ccdc.cam.ac.uk/.

Crystal data for compound **1**: $C_{20}H_{30}O_4$, $M = 334.44$, $a = 10.6243(3)$ Å, $b = 11.7624(3)$ Å, $c = 15.5372(4)$ Å, $\alpha = 90°$, $\beta = 108.1470(10)°$, $\gamma = 90°$, $V = 1845.07(9)$ Å$^3$, $T = 100.(2)$ K, space group $P1211$, $Z = 4$, $\mu$(Cu K$\alpha$) $= 0.658$ mm$^{-1}$, 46654 reflections measured, 7127 independent reflections ($R_{int} = 0.0226$). The final $R_1$ values were 0.0284 ($I > 2\sigma(I)$). The final $wR(F^2)$ values were 0.0967 ($I > 2\sigma(I)$). The final $R_1$ values were 0.0285 (all data). The final $wR(F^2)$ values were 0.0967 (all data). The goodness of fit on $F^2$ was 0.966. Flack parameter $= 0.07(2)$. CCDC: 2015561.

### 4.5. Syntheses

The synthesis procedure and NMR data (Supporting Information Figs. S8−S82) are shown in the Supporting Information

### 4.6. Cell culture and viability

The human liver-derived cell line HepG2 was obtained from the Procell Life Science & Technology Co., Ltd. (Wuhan, China). HepG2 were maintained in DMEM supplemented with 10% ultra-low endotoxin fetal bovine serum, 100 IU/mL penicillin, and 100 IU/mL streptomycin. Cells were incubated at 37 °C in a 5% $CO_2$ humidified atmosphere. Cell viability was measured using the MTT assay. HepG2 cells were seeded in 96-well plates ($1 \times 10^4$ cells per well) for 12 h, and the culture was removed and washed with PBS. Subsequently, each well was added the fresh cell culture medium (10% FBS) with oleic acid (0.5 mmol/L) and fructose (2 mmol/L), and then with or without different concentrations of compound 1 and 2 (1.25, 2.5, 5, and 10 μmol/L) for 48 h. The cell viability was determined by colorimetry with 100 μL of DMEM containing 5 mg/mL MTT at 37 °C for 4 h. After 150 μL DMSO was added for 10 min, the optical density was measured at 490 nm using a microplate reader; complete medium was used as a blank control. Each assay was replicated in five wells, and each experiment was repeated three times.

### 4.7. Analysis of lipids in cells

HepG2 cells in the logarithmic growth phase were seeded in 6-well plates at a density of $2.5 \times 10^5$ cells per well. After 12 h, the cells in the 6-well culture plates were washed with PBS, and the medium (10% FBS) was added, containing oleic acid (0.5 mmol/L)-bovine serum albumin (OA-BSA) and fructose (2 mmol/L) complex in the presence or absence of compounds 1 (2.5, 5, and 10 μmol/L) and positive drug (Atorvastatin, 10 μmol/L) for 48 h. The medium with BSA only was selected as the control. The triglyceride (TG) levels in HepG2 cells were determined in accordance with the instructions of the kits. To analyze the intracellular lipid accumulation, HepG2 cells were stained using oil red O (ORO). Briefly, the cells were washed two or three times with PBS and fixed with 4% paraformaldehyde for 25 min at room temperature. Then, the cells were stained for 40 min in a freshly filtered 0.5% ORO solution at room temperature. The cells were washed using a 60% isopropanol solution for 15−20 s to remove the background staining. The lipid droplet accumulation in HepG2 cells was detected under a microscope. To quantify intracellular lipid accumulation in HepG2 cells, isopropanol (300 μL) was added to each group followed by shaking at room temperature for 15 min. The extracted dye was collected, and a microplate reader monitored its absorbance at 510 nm.

### 4.8. Protein extraction

Total protein was extracted from cells by using lysis buffer (PTM Bio, Hangzhou, China), which consists of 8 mol/L urea and 1% protease inhibitor cocktail. Briefly, the sample was ground with liquid nitrogen into cell powder and then transferred to a centrifuge tube. After that, four volumes of lysis buffer were added to the cell powder, followed by sonication for 3 min on ice using a high-intensity ultrasonic processor (Scientz). The remaining debris was removed by centrifugation at 12,000×*g* at 4 °C for 10 min. Finally, the supernatant was collected and the protein concentration was determined with BCA kit according to the manufacturer's instructions. The protein sample was added with 1 volume of pre-cooled acetone, vortexed to mix, and then added with 4 volumes of pre-cooled acetone, precipitated at −20 °C for 2 h. The precipitate was washed 2 to 3 times with the pre-cooled acetone. The protein sample was then redissolved in 200 mmol/L TEAB and ultrasonically dispersed. Trypsin was added at a 1:50 trypsin-to-protein mass ratio for the first digestion overnight. The sample was reduced with 5 mmol/L dithiothreitol for 30 min at 56 °C and alkylated with 11 mmol/L iodoacetamide for 15 min at room temperature in darkness. Finally, the peptides were desalted by Strata X C18 SPE column (Phenomenex, CA, USA) and vacuum-dried.

### 4.9. Western blotting

This section was performed in accordance with the former reports. Briefly, total proteins from liver tissues were extracted with RIPA lysis buffer (Beyotime, China) containing 1% PMSF (Roche, Switzerland). After centrifugation at 16,099 × *g* at 4 °C for 15 min, the supernatant of the lysate was collected and the protein concentration was detected by BCA method (Solarbio, China). The proteins of samples were released by boiling in SDS loading buffer, separated on SDS−PAGE gels and transferred onto the PVDF membrane (0.22 μm, Merck KGaA, Germany). After blocked with 5% nonfat-milk for 2 h at room temperature, the membranes were incubated with primary antibodies overnight at 4 °C, including Bckdk (ab128935, Abcam), Cpt-1 (ab234111, Abcam), Ppar-$\alpha$ (ab178865, Abcam), Acaca (ab45174, Abcam), Scd-1 (#2438, CST), Srebp-1c (AF6283, Affinity), Notch3 (AF7548, Affinity), Pgc-1 (AF5395, Affinity), and $\beta$-actin (AF7018, Affinity). After washing by TBST three times (10 min each), the membrane was developed with a secondary antibody. The antibodies were diluted according to the manufacturer's instructions. Finally, immunoreactive protein signals were spotted by the Odyssey Infrared Imaging System. $\beta$-actin served as an internal loading control.

### 4.10. Zebrafish maintenance

The transgenic zebrafish line Tg (cy3: EGFP) was sourced from Zebrafish Drug Screening Platform of Shandong Academy of Sciences (Jinan, China). The adult zebrafish were housed in an aquaculture facility with 14 h light and 10 h darkness photoperiod at 28 °C. Before mating, adult male and female zebrafish were separated in a breeding tank at a ratio of 2:1. After the light on the next morning, embryos were generated by natural mating. The embryos were collected within 1 h of spawning and rinsed thrice with fresh water. The clean embryos were maintained in medium (5 mmol/L NaCl, 0.17 mmol/L KCl, 0.4 mmol/L $CaCl_2$, and 0.16 mmol/L $MgSO_4$) within the incubator at the same temperature and photoperiod. All the experimental procedures were carried out under the approval of the Biology Institute, Guizhou Medical University Animal Ethics Committee (Approval number: SYXK 2023-0002).

### 4.11. Hepatoprotective activity assay

The well-developed zebrafish larvae at 5 days post-fertilization (dpf) were randomly transferred to a 6-well plate with 20 larvae per well. To test the hepatoprotective activity of compound **1**, zebrafish were treated with egg yolk and fructose (1:1) at a concentration of 0.1 g/100 mL for 48 h. Following the treatment, the medium was removed and the zebrafish were washed with fresh water. Subsequently, the zebrafish larvae at 7 dpf were added to the fresh medium with different concentrations of compound **1** (2.5, 5, and 10 μmol/L) and positive drug (Atorvastatin, 10 μmol/L) for 24 h. Those exposed solely to egg yolk and fructose were served as the model group. The zebrafish maintained in fresh fish water without any treatment were utilized as the blank control. At 8 dpf, the larvae were anesthetized with tricaine (Sigma) and immobilized in 3% methylcellulose (Beyotime, Shanghai, China), and then were observed and photographed under a fluorescence microscope (SZX16; Olympus, Tokyo, Japan).

### 4.12. Oil red O staining

To prepare the oil red O working solution, 0.5 g of oil red O powder (Sigma) is fully dissolved in 100 mL of isopropanol and stored at 4 °C in the dark. Before use, the stock solution was diluted with distilled water at a ratio of 3:2 (*v*/*v*), and then was thoroughly filtered through the 0.22 mm micropore filter to obtain the working solution without sediment. After treatment, zebrafish larvae were fixed in 4% paraformaldehyde at 4 °C overnight, followed by dehydration in a sequential gradient of 25%, 50%, 75%, and 100% propylene glycol/phosphate-buffered saline (PBS) for 10 min, respectively. The larvae were then stained with the oil red O working solution overnight at room temperature, and rehydrated in 100%, 75%, 50%, and 25% propylene glycol/PBS. The pathological changes were observed using the stereomicroscope. The staining of lipid drops by oil red O was quantified using ImageJ to obtain the integrated optical density (IOD).

## Acknowledgments

This research was financially supported by the National Natural Science Foundation of China (22361008, 32270413, 22061008, 82160808), Excellent Young Talents Plan of Guizhou Medical University (2023, No.106, China), Guizhou Provincial Major Scientific and Technological Program ([2024]015, China), Guizhou Science and Technology Innovation Talent Team (No. QKHPTRC-CXTD[2022]007, China), 2025 Independent Research Project of State Key Laboratory of Discovery and Utilization of Functional Components in Traditional Chinese Medicine, Guizhou Medical University (GMUSKL-202503, China), Science and Technology Foundation of Guizhou Province (No. ZK[2021]-039, QKHJC-ZD[2025]027, China), the State Key Laboratory of Functions and Applications of Medicinal Plants, Guizhou Medical University (No. FAMP202102K, China).

## Author contributions

Chunmao Yuan: Conceptualization, Investigation, Funding acquisition, Writing, review & editing. Zhao Liu: Investigation, Writing review & editing. Lei Huang: Investigation, Writing review & editing. Yanrong Zeng: Investigation. Chunxiang Mei: Investigation, Writing review & editing. Yanmei Li: Investigation, Writing review & editing. Yang Chen: Data curation, Formal analysis, Validation. Hongji Wang: Investigation and Validation. Lan Yang: Investigation and Validation. Xiaojiang Hao: Conceptualization, Funding acquisition, Supervision, Writing, review & editing. Shuzhong He: Conceptualization, Funding acquisition, Supervision, Writing, review & editing.

## Conflicts of interest

The authors declare no conflicts of interest.

## Appendix A. Supporting information

Supporting information to this article can be found online at https://doi.org/10.1016/j.apsb.2025.10.008.

## References

1. Brunt EM, Wong VS, Nobili V, Day CP, Sookoian S, Maher JJ, et al. Non-alcoholic fatty liver disease. *Nat Rev Dis Primers* 2015;**1**:15080.
2. Paternostro R, Trauner M. Current treatment of non-alcoholic fatty liver disease. *J Intern Med* 2022;**292**:190−204.
3. Kim M, Hwang I, Pagire HS, Pagire SH, Choi W, Choi WG, et al. Design, synthesis, and biological evaluation of new peripheral 5-HT2A antagonists for nonalcoholic fatty liver disease. *J Med Chem* 2020;**63**:4171−82.
4. Newman DJ, Cragg GM. Natural products as sources of new drugs over the nearly four decades from 01/1981 to 09/2019. *J Nat Prod* 2020;**83**:770−803.
5. Yin S, Liu Z, Shen JJ, Xia YW, Wang WH, Gui PY, et al. Chimeric natural products derived from medermycin and the nature-inspired construction of their polycyclic skeletons. *Nat Commun* 2022;**13**:5169.
6. Ueoka R, Sondermann P, Leopold Messer S, Liu YZ, Suo R, Bhushan A, et al. Genome-based discovery and total synthesis of janustatins, potent cytotoxins from a plant-associated bacterium. *Nat Chem* 2022;**14**:1193−201.
7. Zheng Y, Teng LL, Zhou TT, Liu ZW, Guo K, Li H, et al. Discovery and total synthesis of a new class of minor immunosuppressive plant sesterterpenoids. *Angew Chem Int Ed* 2025;**64**:e202421497.
8. Yang XW, Grossman RB, Xu G. Research progress of polycyclic polyprenylated acylphloroglucinols. *Chem Rev* 2018;**118**:3508−58.
9. Ciochina R, Grossman RB. Polycyclic polyprenylated acylphloroglucinols. *Chem Rev* 2006;**106**:3963−86.
10. Guo Y, Huang F, Sun WG, Zhou Y, Chen CM, Qi CX, et al. Unprecedented polycyclic polyprenylated acylphloroglucinols with anti-

alzheimer's activity from st. John's wort. *Chem Sci* 2021;**12**: 11438−46.
11. Ye YS, Li WY, Du SZ, Yang J, Nian Y, Xu G. Congenetic hybrids derived from dearomatized isoprenylated acylphloroglucinol with opposite effects on Cav3.1 low voltage-gated $Ca^{2+}$ channel. *J Med Chem* 2020;**63**:1709−16.
12. El Hamdaoui Y, Zheng F, Fritz N, Ye L, Tran MA, Schwickert K, et al. Analysis of hyperforin (St. John's wort) action at TRPC6 channel leads to the development of a new class of antidepressant drugs. *Mol Psychiatr* 2022;**27**:5070−85.
13. Duan Y, Sun W, Li Y, Shi Z, Li L, Zhang Y, et al. Spirohypertones A and B as potent antipsoriatics: tumor necrosis factor-$\alpha$ inhibitors with unprecedented chemical architectures. *Acta Pharm Sin B* 2024;**14**: 2646−56.
14. Yuan CM, Zeng YZ, Huang L, Mou Y, Jin J, Yi P, et al. Hymoins A−C, three unusual polycyclic polyprenylated acylphloroglucinols with lipid-lowering activity from *Hypericum monogynum*. *Chin Chem Lett* 2025;**36**:109859.
15. Huang L, Zhang ZZ, Li YN, Yi P, Gu W, Yang J, et al. Hypersampones A−C, three nor-polycyclic polyprenylated acylphloroglucinols with lipid-lowering activity from *Hypericum sampsonii*. *Org Lett* 2022;**24**: 5967−71.
16. Shimizu Y, Shi SL, Usuda H, Kanai M, Shibasaki M. Catalytic asymmetric total synthesis of ent-hyperforin. *Angew Chem Int Ed* 2010;**49**:1103−6.
17. Wen S, Boyce JH, Kandappa SK, Sivaguru J, Porco JA. Regiodivergent photocyclization of dearomatized acylphloroglucinols: asymmetric syntheses of (−)-nemorosone and (−)-6-epi-garcimultiflorone A. *J Am Chem Soc* 2019;**141**:11315−21.
18. Biber N, Mows K, Plietker B. The total synthesis of hyperpapuanone, hyperibone L, epi-clusianone and oblongifolin A. *Nat Chem* 2011;**3**: 938−42.
19. Wen S, Boyce JH, Kandappa SK, Sivaguru J, Porco JA. Regiodivergent photocyclization of dearomatized acylphloroglucinols: asymmetric syntheses of (−)-nemorosone and (−)-6-epi-garcimultiflorone A. *J Am Chem Soc* 2019;**141**:11315−21.
20. Sparling BA, Moebius DC, Shair MD. Enantioselective total synthesis of hyperforin. *J Am Chem Soc* 2013;**135**:644−7.
21. Ng S, Howshall C, Ho TN, Mai BK, Zhou Y, Qin C, et al. Catalytic prenyl conjugate additions for synthesis of enantiomerically enriched PPAPs. *Science* 2024;**386**:167−75.
22. Plesniak MP, Huang HM, Procter DJ. Radical cascade reactions triggered by single electron transfer. *Nat Rev Chem* 2017;**1**:77.
23. Zhang L, Sun J, Kozmin SA. Gold and platinum catalysis of enyne cycloisomerization. *Adv Synth Catal* 2006;**348**:2271−96.
24. Michelet V, Toullec PY, Genêt JP. Thiophene-based conjugated acetylenic polymers with dual active sites for efficient co-catalyst-free photoelectrochemical water reduction in alkaline medium. *Angew Chem Int Ed* 2008;**120**:4338−86.
25. Obradors C, Echavarren AM. Gold-catalyzed rearrangements and beyond. *Acc Chem Res* 2014;**47**:902−12.
26. Hu Y, Bai M, Yang Y, Zhou QH. Metal-catalyzed enyne cycloisomerization in natural product total synthesis. *Org Chem Front* 2017; **4**:2256−75.
27. Mohapatra DK, Pramanik C, Chorghade MS, Gurjar MK. A short and efficient synthetic strategy for the total syntheses of (*S*)-(+)- and (*R*)-(−)-plakolide A. *Eur J Org Chem* 2007;**30**:5059−63.
28. Nieto Oberhuber C, Muñoz MP, López S, Jiménez Núñez E, Nevado C, Herrero Gómez E, et al. Gold(I)-catalyzed cyclizations of 1,6-enynes: alkoxycyclizations and exo/endo skeletal rearrangements. *Chem Eur J* 2006;**12**:1677−93.
29. Li D, Yang J, Liu B, Gong J, Yang Z. Synthesis of desacyl furanmonogones A and B. *Org Lett* 2021;**23**:4532−7.
30. Snider BB. Manganese (III)-based oxidative free-radical cyclizations. *Chem Rev* 1996;**96**:339.
31. Mondal M, Bora U. Recent advances in manganese (III) acetate mediated organic synthesis. *RSC Adv* 2013;**3**:18716−54.
32. Chisholm MH, Huffman JC, Tatz RJ. Dimolybdenum compound (*iso*-PrO)3 Mo.tplbond. Mo($CH_2$Ph)2(*O-iso*-Pr)(PMe3): the first example of a compound containing a triple bond uniting three- and four-coordinate molybdenum atoms and the observation of phosphine-promoted, reversible benzyl-alkoxy migrations at the (M.tplbond. M)$^{6+}$ center. *J Am Chem Soc* 1984;**106**:5384−538.
33. Dombroski MA, Kates SA, Snider BB. Manganese (III)-based oxidative free-radical tandem and triple cyclizations. *J Am Chem Soc* 1990;**112**:2759−67.
34. Snider BB, Merritt JE, Dombroski MA, Buckman BO. Solvent effects on manganese (III)-based oxidative free-radical cyclizations: ethanol and acetic acid. *J Org Chem* 1991;**56**:5544−53.
35. Yang D, Gu S, Yan YL, Zhu NY, Cheung KK. Highly enantioselective atom-transfer radical cyclization reactions catalyzed by chiral Lewis acids. *J Am Chem Soc* 2001;**123**:8612−3.
36. Friestad GK, Shen Y, Ruggles EL. Enantioselective radical addition to *N*-acyl hydrazones mediated by chiral Lewis acids. *Angew Chem Int Ed* 2002;**114**:3140−3.
37. Powell LH, Docherty PH, Hulcoop DG, Kemmitt PD, Burton JW. Oxidative radical cyclisations for the synthesis of $\gamma$-lactones. *Chem Commun* 2008;**14**:2559−61.
38. Logan AWJ, Parker JS, Hallside MS, Burton JW. Manganese (III) acetate mediated oxidative radical cyclizations toward vicinal all-carbon quaternary stereocenters. *Org Lett* 2012;**14**:2940−3.
39. Powell LH, Docherty PH, Hulcoop DG, Kemmitt PD, Burton JW. Oxidative radical cyclisations for the synthesis of $\gamma$-lactones. *Chem Commun* 2008;**14**:2559−61.
40. Logan AWJ, Parker JS, Hallside MS, Burton JW. Manganese (III) acetate mediated oxidative radical cyclizations toward vicinal all-carbon quaternary stereocenters. *Org Lett* 2012;**14**:2940−3.
41. Harrison SA, Bedossa P, Guy CD, Schattenberg JM, Loomba R, Taub R, et al. Retrospective AI-based measurement of NASH histology (AIM-NASH) analysis of biopsies from Phase 2 study of Resmetirom confirms significant treatment-induced changes in histologic features of non-alcoholic steatohepatitis. *J Hepatol* 2022;**77**:S711−2.
42. Jia G, Aroor AR, Martinez-Lemus LA, Sowers JR. Fructose and glucose combined with free fatty acids induce metabolic disorders in HepG2 cell: a new model to study the impacts of high-fructose/sucrose and high-fat diets *in vitro*. *Mol Nutr Food Res* 2016;**60**:909−21.
43. Van KA, Verschuren L, van den Hoek AM, Verheij J, Morrison MC, Li K, et al. Transcriptomic profiling of induced steatosis in human and mouse precision-cut liver slices. *Sci Data* 2023;**10**:304.
44. Samuel VT, Shulman GI. Nonalcoholic fatty liver disease as a nexus of metabolic and hepatic diseases. *Cell Metab* 2017;**27**: 22−41.
45. Guo W, Li Z, Anagnostopoulos G, Kong WT, Zhang S, Chakarov S, et al. Notch signaling regulates macrophage-mediated inflammation in metabolic dysfunction-associated steatotic liver disease. *Immunity* 2024;**57**:2310−27.
46. Roth Flach RJ, Bollinger E, Reyes AR, Laforest B, Kormos BL, Liu S, et al. Small molecule branched-chain ketoacid dehydrogenase kinase (BDK) inhibitors with opposing effects on BDK protein levels. *Nat Commun* 2023;**14**:4812.
47. Linghu L, Zong W, Liao Y, Chen Q, Meng F, Wang G, et al. Herpetrione, a new type of PPAR$\alpha$ ligand as a therapeutic strategy against nonalcoholic steatohepatitis. *Research* 2023;**6**:276.
48. Pajvani UB, Qiang L, Kangsamaksin T, Kitajewski J, Ginsberg HN, Accili D. Inhibition of notch uncouples Akt activation from hepatic lipid accumulation by decreasing mTorc1 stability. *Nat Med* 2013;**19**: 1054−60.
49. Auguet T, Bertran L, Binetti J, Aguilar C, Martínez S, Guiu Jurado E, et al. Hepatocyte Notch signaling deregulation related to lipid metabolism in women with obesity and nonalcoholic fatty liver. *Obesity* 2020;**28**:1487−93.
50. Grenier Larouche T, Kwee LC, Deleye Y, Leon Mimila P, Walejko JM, McGarrah RW, et al. Altered branched-chain $\alpha$-keto acid metabolism

is a feature of NAFLD in individuals with severe obesity. *JCI Insight* 2022;**7**:e159204.
51. Guo YX, Tan JY, Xiong W, Chen SZ, Fan LP, Li YC. Notch3 promotes 3T3-L1 pre-adipocytes differentiation by up-regulating the expression of LARS to activate the mTOR pathway. *J Cell Mol Med* 2020;**4**: 1116−27.
52. Gosis BS, Wada S, Thorsheim C, Li K, Jung S, Rhoades JH, et al. Inhibition of nonalcoholic fatty liver disease in mice by selective inhibition of mTORC1. *Science* 2022;**15**:376.
53. Sapp V, Gaffney L, Eau Claire SF, Matthews RP. Fructose leads to hepatic steatosis in zebrafish that is reversed by mechanistic target of rapamycin (mTOR) inhibition. *Hepatology* 2014;**60**:1581−92.